LANGMUIR

Subscriber access provided by Kaohsiung Medical University

Biological and Environmental Phenomena at the Interface

"V-shape" molecular configuration of wax esters of jojoba oil in a Langmuir film model

Benjamín Caruso, M. Florencia Martini, Mónica Pickholz, and Maria Angelica Perillo

Langmuir, **Just Accepted Manuscript** • DOI: 10.1021/acs.langmuir.8b00693 • Publication Date (Web): 31 May 2018

"V-shape" molecular configuration of wax esters of jojoba oil in a Langmuir film model

Benjamín Caruso[1], M. Florencia Martini[2], Mónica Pickholz[3] and María A. Perillo[1]*

[1] *Universidad Nacional de Córdoba, Facultad de Ciencias Exactas, Físicas y Naturales. Departamento de Química, Cátedra de Química Biológica. Córdoba, Argentina and CONICET, Instituto de Investigaciones Biológicas y Tecnológicas (IIByT). Córdoba, Argentina. Av.Velez Sarsfield 1611, 5016 Córdoba, Argentina.*

[2] *Universidad de Buenos Aires. Facultad de Farmacia y Bioquímica. Cátedra de Química Medicinal. Buenos Aires, Argentina and CONICET-Universidad de Buenos Aires. Instituto de la Química y Metabolismo del Fármaco (IQUIMEFA). Buenos Aires, Argentina. Junín 956 SS, 1113 Buenos Aires, Argentina.*

[3] *Universidad de Buenos Aires. Facultad de Ciencias Exactas y Naturales. Departamento de Física. Buenos Aires, Argentina and CONICET - Universidad de Buenos Aires. Instituto de Física de Buenos Aires (IFIBA). Buenos Aires, Argentina. Intendente Güiraldes 2160, Pabellon 1, Ciudad Universitaria Universidad de Buenos Aires, C1428BFA CABA, Argentina.*

*Corresponding author

e-mail: mperillo@unc.edu.ar

Abstract

The aim of the present work was to understand the interfacial properties of a complex mixture of wax esters (WEs) obtained from Jojoba oil (JO). Previously, based on molecular area measurements, a hairpin structure was proposed as the hypothetical configuration of WEs allowing their organization as compressible monolayers at the air-water interface. In the present work we contributed with further experimental evidences by combining surface pressure (π), surface potential (ΔV) and PM-IRRAS measurements of JO monolayers and molecular dynamic simulations (MD) on a modified JO model. WEs, both self-assembled in Langmuir films. Compression isotherms exhibited a $\pi_{lift\text{-}off}$ at 100Å^2/molecule mean molecular area ($A_{lift\text{-}off}$) and a collapse point at π_c~2.2mN/m and A_c~77Å^2/molecule. The ΔV profile reflected two dipolar reorganizations one of them at $A>A_{lift\text{-}off}$ due to the release of loosely bound water molecules and another one at $A_c<A<A_{lift\text{-}off}$ possibly due to reorientations of a more tightly bound water population. This was consistent with the maximal SP value that was calculated according to a model that considered two populations of oriented water and resulted very close to the experimental value. The orientation of the ester group that was assumed in that calculation was coherent with the PM-IRRAS behavior of the carbonyl group with the C=O oriented towards the water and the C-O oriented parallel to the surface and were in accordance with their orientational angles (~45° and ~90°, respectively) determined by MD simulations. Taken together the present results confirm a "V-shape" rather than a hairpin configuration of WEs at the air-water interface.

Key words: wax esters, jojoba oil, Langmuir films, molecular packing, surface electrostatics, PM-IRRAS, molecular dynamics.

Abbreviations: A_c, Molecular area at collapse of monolayer; A_{min}, Minimal mean molecular area; BP, Behenyl palmitoleate; DBI, Double bond index; D(φ), angle density distribution ; EDP, Electron density profile; EE, Eicosanoyl eicosanoate; HLB, Hydrophylic/lipophilic balance; HP, Hexadecyl palmitate; JO, Wax ester fraction of jojoba oil; K, Compressibility modulus; LCGE, long chain, glycerol-based esters; Mma, Mean molecular area; O, Triglyceride fraction of olive oil; P(θ), Probability density of vector angles; $P_{iso}(\theta)$, Probability of isotropic vector angle distribution; π, Lateral surface pressure; $\pi_{C,}$ Lateral surface pressure at the collapse of monolayer; S, Triglyceride fraction of soybean oil; SA, Stearic acid; S_{CD}, Order parameter of C-D vectors; SS, Stearyl stearate; Tm, Melting point; TG, Triglyceride; TO, Triolein; TS, Tristearin; W, Triglyceride fraction of walnut oil; WE, Wax ester; θ, Vector ´s angle relative to the normal to the interface; ν_{max}, Wavenumber of maximum absorption in PM-IRRAS; ΔR/R, Normalized signal intensity in PM-IRRAS; ΔV_0, Area independent electrostatic surface potential; ΔV_{D-F}, Electrostatic surface potential calculated using the Demchak-Fort model; ΔV_{max}, Maximum electrostatic surface potential that can be achieved in a non-collapsed monolayer; ΔV, Electrostatic surface potential.

Introduction

Many natural waxes are lipid mixtures whose major components are long chain monoester molecules (called wax esters, WE) consisting on a fatty acid esterified with a long chain primary alcohol. WE are highly abundant in nature providing energy and carbon storage [1-2], protection of plants and animals against desiccation or external stresses [3-6], buoyancy and others (refs in [7-8]). A widely studied natural wax is found in *Simmondsia chinensis* seeds. This wax is commonly known as "jojoba oil" as, unlike most natural waxes, it is found in a liquid state at ambient temperature. Such property, together with its extraordinary high thermal and oxidative stabilities, have made jojoba oil a common component in cosmetics and hair care products, as well as a feedstock for lubricant and additive applications, as the viscosity index of jojoba oil is much higher than that of petroleum oil (see ref. in [9-10])

Moreover, WE biosynthesis was successfully accomplished in transgenic *Arabidopsis* seeds expressing jojoba embryo wax synthase [11]. This is highly relevant from a technological viewpoint since in light of diminishing resources of fossil hydrocarbons, the use of oilseed crops may contribute for sustainable production of high value chemicals for industry [12].

In order to understand many of the biological functions of WE and design new industrial formulations that include them, the interfacial properties of their phase-separated structures should be considered, which implies evaluating their interfacial stability. However, studies on WE interfacial behavior are scarce and has been for long focused on WEs with saturated chains (thus in solid state) which tend to aggregate at the interface [13-14]. Only recently, the interfacial (air-water) properties of films of meibonian WE has begun to receive attention [15-16]. These studies highlighted the role of the physical state in determining WE monolayer stability: liquid but not solid WE molecules would be able to spread over an air-water interface. Previously, we evaluated the ability of the WE fraction of jojoba oil (hereafter termed "JO") to form monomolecular layers [9, 17] and associated it with the hypothetical configuration acquired by the long alkyl chains at the air-water interface. Thus, we [17]and Paananen et al. [15] proposed that, in the solid phase, WEs formed multilayer films where most molecules exhibited a linear configuration, whereas in the fluid state they adopt a hairpin-like structure with an amphipathic-driven orientation and spread on interfaces leading to form compressible monolayers. However, such hypothetic configurations are supported only by molecular area measurements.

The low collapse pressure and large minimal mean molecular area observed in WE monolayers have been interpreted to be a consequence of the low hydrophilic/lipophylic balance (HLB) due to a polar head group too small compared with the volume occupied by the bulky long and unsaturated hydrocarbon-chains. Furthermore, the geometry of the monoester polar group might difficult the orientation of the two hydrocarbon chains parallel between one another and in the perpendicular direction with respect to the interface [9]. Teixeira et al. [18] also pointed out the importance of the low HLB as a destabilizing factor for the formation of monolayers of the long chain ester stearyl stearate (SS) (see below). However, it was early in the monolayer literature that the constraints for the formation of stable monolayers of WE were analyzed. Adam [13] reported hexadecyl palmitate (HP) films as solid and with a molecular area of about 41 $Å^2$. Although the relation between mean molecular area (Mma) and lateral surface pressure (π) could not be accurately mapped, they suggested an ester configuration that implied the alkyl chain to bend completely so as to lie nearly vertically along-side the acidic chain. Later on, from π/Mma and ΔV/Mma isotherms of a variety of long chain esters, Alexander & Schulmann [14] also suggested that in the case of HP, the ester group could acquire such a configuration that allowed the alkyl and acid chains to be parallel, with a lateral adhesion that stabilized a "hairpin-like" structure. This resulted on a condensed film that collapsed at very low lateral pressure (0.4 mN/m), and 40 $Å^2$/molecule. According to these authors, this bending of the alkyl chain resulted on an apparent dipole moment of the ester group of approximately zero.

In accordance with these findings, from π/Mma isotherms, BAM and AFM analyses on SS, Teixeira et al. [18] concluded that, due to its low hydrophilicity, pure SS did not form a stable monolayer at the air–water interface. Instead, it organizes into an asymmetric multilayer (or duplex film) where in a first layer SS adopts a U configuration to orient the polar group towards the water subphase, while in the upper layers SS adopts a linear configuration in order to maximize laterally both the polar and hydrophobic interactions. Thus, although these authors could not observe a stable monolayer, their interpretation implies the possibility of the ester group to bend and adopt a hairpin configuration. Furthermore, when mixed with stearic acid (SA) or tristearin (TS) in the monolayer regime, the linear variation of the mean molecular area (Mma) of these mixtures at constant lateral pressure is compatible with the additive rule of molecular areas of pure components, i.e. Mma = 20 $Å^2$/molecule for SA, 57 $Å^2$/molecule for TS and 38 $Å^2$/molecule for SS. This strongly supports their hypothesis of

hairpin-like configuration for SS molecules, laterally anchored by the SA or the TS chains. Similarly, in the case of the mixtures of JO with triglycerides (TG) [9], we observed a negative deviation of the Mma of the mixtures at all proportions. This fact, together with an increasing collapse pressure (π_C) with increasing TG content, indicated a high interfacial miscibility of these compounds and the possibility that JO-containing monolayers can remain stable at π above the π_C of pure JO, as it occurs with SS.

Taking into account that JO is a mixture of esters with different hydrocarbon chain lengths, here, we firstly evaluated the possibility to describe the surface packing properties of JO monolayers through compositional average parameters. Then, we analyzed the configuration of JO molecules at the air-water interface by comparing surface potential and IR spectroscopy (PM-IRRAS) measurements of JO with ~~atomic scale~~ molecular dynamics simulations of a representative wax ester.

Materials and methods

Materials

Solvents used were of analytical grade. The WE fraction of jojoba oil (JO) was obtained and its acyl and alkyl moieties composition were characterized as detailed previously [9]. According to GC-mass spectrometry analyses after ester alkaline hydrolysis, JO is 99% composed of monounsaturated acyl moieties, the saponifiable fraction being more rich in cis-11-eicosenoic (20:1) acid (72.5%), followed by 18:1 (10.1%) and 22:1 (14.8%). On the other hand, GC-mass spectrometry analysis of the unsaponifiable fraction arose that JO presents similar amounts of the fatty alcohols (derived from alkyl moieties) 20:1 (42%) and 22:1 (48%). A 9% of cis-15-tetracosenol (24:1) is also present. Other acyl and alkyl moieties are present in small proportions and the overall compositional information was used to calculate a JO mean molecular mass MMM = 608 [9]. Similarly and following the rational applied in a previous study on monolayers composed of complex mixtures of triglycerides from vegetable oils [19], other mean parameters that describe average molecular properties were calculated here to describe JO. This was an attempt to evaluate how acyl chain composition can determine the collective behavior of the complex molecular mixture. For example, the Double Bond Index (DBI) was used to describe the acyl chain unsaturation level and was calculated according to Eq.1:

$$DBI = \sum \frac{(UF.DB)}{100} \qquad (1)$$

where UF is the mole percent composition of each unsaturated fatty acyl or alkyl chain and DB is its respective number of double bonds. The value of DBI for JO calculated in the present work was interpolated in the DBI vs. Mma plot defined for TGs in a previous work [19], Fig. 1b. This was aimed at testing the hypothesis that *DBI* can describe the average behavior of widespread complex mixtures such as TGs and JO, and that WE adopting a hairpin-like structure when organized in Langmuir films, should exhibit surface properties that correlate with those of TGs.

Monomolecular layers at the air-water interface

Monomolecular layers were prepared and monitored essentially as described previously [9, 20-22]. The equipment used was a Minitrough II (KSV Instruments Ltd, Finland). Between 10 and 20 μl of a $CHCl_3$:MeOH (2:1) solution of JO (1 mM) was spread on an unbuffered aqueous surface (24000 mm^2) at room temperature (24°C ± 0.5°C). About 5 min. were allowed for the evaporation of the solvent. Lateral surface pressure (π) was measured by the Wilhelmy plate method. Shear may influence isotherm determinations. This phenomenon was discarded by placing the Wilhelmy plate in two perpendicular directions observing no effects on the registered isotherms. Before each experiment the trough was rinsed and wiped with 70 % ethanol and several times with bidistilled water. The absence of surface-active compounds in the pure solvents and in the subphase solution (bidistilled water) was checked before each run by reducing the available surface area to less than 10% of its original value after 5 minutes were allowed for the adsorption of possible impurities that might have been present in trace amounts.

Surface pressure (π), compressibility modulus (K) and surface potential (ΔV) vs mean molecular area (Mma) isotherms

Monolayers were compressed and expanded at two constant rates, 7.5 and 37.5 $mm^2.min^{-1}$, which led to identical results. Mma at varying π was calculated dividing surface area by the number of molecules spread on the interface. K was calculated for each isotherm according to Eq.2:

$$K = -(Mma)_{\pi} \cdot \left(\frac{\delta\pi}{\delta Mma}\right)_T \qquad (2)$$

where Mma_{π} is the molecular area at π.

The surface potential (ΔV) of a monolayer is defined as the difference between the electric potentials, relative to the air phase, of a subphase covered with a monolayer and the

same "clean" subphase. It arises as a consequence of the dipolar moments of the molecules forming the monolayer and the water molecules from subphase bound and properly oriented at the interface. In the case of ionized monolayers, the ionic double layer generated between the lipid headgroups and the subphase electrolytes also contribute to ΔV. Here, this factor is neglected as the monolayer almost lacks ionizable groups in the experimental conditions set, *i..e.*, free fatty acid content <0.01 mole fraction, pure water subphase and 24 ºC.

The vibrating plate technique was used for determining ΔV, where the potential difference between two plates of a parallel plate capacitor is measured. By vibrating the plate at the air phase, a displacement current is generated, which can be offset by applying an external depolarization voltage until a null potential difference is registered between the plates. This external potential represents the contact potential and corresponds to ΔV .

Calculations of the magnitude of dipole moments of the monolayer forming molecules were calculated according to the Helmholtz model (Eq.3) which considers that a parallel plate capacitor covers a layer of uniformly distributed dipoles:

$$\Delta V = \frac{\mu_{\perp}}{Mma.\varepsilon_r.\varepsilon_0} \qquad (3)$$

where ε_r and ε_0 represent the relative dielectric constant and the vacuum permittivity, respectively, and $\mu_{\perp}$ is the apparent dipole moment (i.e. the resultant of the perpendicular components of all the dipoles oriented at the interface), ε_r is considered a macroscopic magnitude, which has led to various interpretations concerning the value it should assume, including the possibility of being disaggregated in order to represent different environments for the different contributions to $\mu_{\perp}$, namely, headgroups, oriented water, hydrophobic tails. Furthermore, there exist models that describe the monolayer as a two- or three-plates capacitor, e.g. Vogel-Möbius and Demchak-Fort models, respectively [23]. The ΔV calculated according the latter model (ΔV_{D-F}) is described by Eq.4:

$$\Delta V_{D-F} = \frac{1}{Mma\ \varepsilon_0}\left(\frac{\mu_1}{\varepsilon_1} + \frac{\mu_2}{\varepsilon_2} + \frac{\mu_3}{\varepsilon_3}\right) 3.33 \times 10^{-30} C\ m \qquad (4)$$

where Mma is expressed in m^2. The following values where assigned to the constants (taken from [24]:

- ε_0 = 8.85 x 10^{-12} F·m^{-1}
- $\frac{\mu_1}{\varepsilon_1}$ = -65 mD, represents the ratio between the vertical component of the dipole moment due to the water molecules orientation induced by the presence of the monolayer (μ_1) and the dielectric constant of the media surrounding them (ε_1),

- μ_2=1110 mD, is the normal component of the dipole moment of the hydrophilic group (ester) localized in a medium of a dielectric constant ε_2=6 .4
- μ_3 is the vertical component of the dipole moment due to the hydrocarbon chains (it is assumed that each terminal methyl group contribute with 330 mD) and ε_3=2.8 is the dielectric constant at the air-monolayer interface,

To estimate the ΔV of JO, 2.μ_3 was applied.

Polarization Modulation Infrared Reflection-Absorption Spectroscopy (PM-IRRAS)

PM-IRRAS was performed with a KSV PMI 550 PM-IRRAS (KSV Instruments Ltd., Finland) mounted on a KSV Minitrough and compression isotherms were performed as described above. Spectra were collected with a resolution of 8 cm^{-1}, at 100 kHz modulating frequency and a variable delay in the wavelength (λ). The incidence angle was 80° and the maximum retardation wavelength was 1500 cm^{-1} with a gap of 0.55λ. These parameters enabled a high resolution IR spectrum to be recorded within the 1500 and 3000 cm^{-1} wavenumber range in which most signals from the ester and methylene group appeared. A positive-oriented band indicates a transition moment occurring preferentially in the plane of the surface, while a negative downward-oriented band reveals an orientation preferentially perpendicular to the surface [25-26].

Computational details

We performed atomic-scale molecular dynamics simulations of single-component lipid monolayers comprised of a WE representative of JO composition (11-cis eicosenoyl 11-cis-eicosenoate, EE) in aqueous solution for two molecular packing conditions. The simulated systems consist of a periodically replicated cell, divided into two monolayers with 31 or 25 EE molecules, corresponding to 80 and 100 $Å^2$/molecule densities, respectively. The monolayers are separated by a slab containing 8100 water molecules. The system is effectively periodic in 3D and no interactions are expected across the *z* direction (normal to the interfaces) because of the large vacuum region (18 nm), as depicted in Scheme.1.

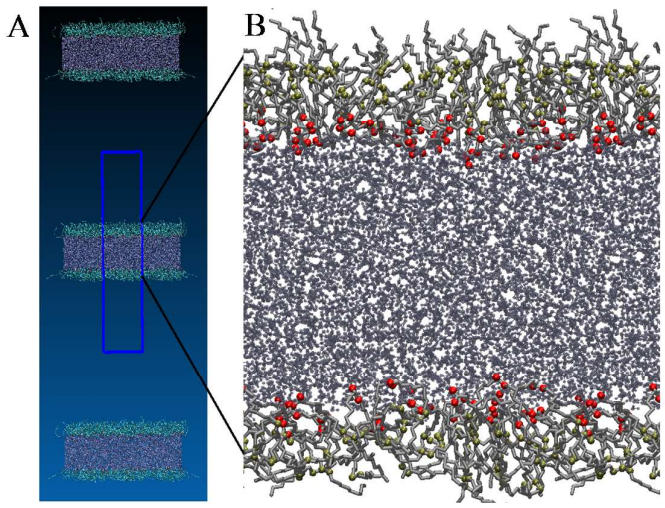

Scheme. 1. A. Simulation box showing periodic boundary condition in z and x axis, B. Zoom effect on monolayers and water system. Water molecules are in ice-blue, hydrocarbon chains in silver and licorice representation, Oxygen atoms of EE are in red and CPK representation, double bounds of hydrocarbon tails are in ochre and CPK representation.

The simulation geometry is similar to that applied previously ([27] and refs. therein) and has been used in many studies [28-31]. The size of the simulation cell was kept constant to accommodate the EE molecules on each interface (fixed area per lipid of 80 Å^2 and 100 Å^2 [32-34] and *Lz*=26 nm, to ensure that interactions across the z axis where negligible for each surface density considered at a fixed amount of water molecules.

The molecular dynamics simulations were performed by GROMACS 4.0 software package [35-37]. The GROMOS-96 53a6 force field [38] was used. Methylene and methyl groups of lipid molecules were treated as united atom type. Water was modeled using the simple point charge (SPC) model [39]. The electrostatic interactions were handled with the SPME version of the Ewald sums [40-41]. The settings for the SPME method were a real space cut-off of 1.5 nm, a grid spacing of 0.24 nm and a cubic interpolation. In all the simulations, the van der Waals interactions were cut off at 1.5 nm. The simulations were carried out in the NVT ensemble using the Berendsen thermostat [42]. The whole system was coupled to a temperature bath with a reference temperature of 300 K and a relaxation constant of 0.1 ps. No constraints were used for the bonds. The time step for the integration of the equation of motion was 1 fs. The nonbonded list was updated every 10 steps.

The simulated systems were built in a tetragonal box, using the Packmol package [43]. To release steric clashes we performed a simulation with steepest descent algorithm and continued by conjugated gradient algorithm. Prior to the production run, a series of six equilibration steps of 5 ns each were performed upgrading the temperature progressively.

The ground-state geometry of EE was optimized within the density functional theory with use of the B3LYP functional and 6-31G* basis set[44]. The partial atomic charges were obtained through a single point HF/6-31G*using Gaussian [45]. and the Merz–Singh–Kollman protocol

[46-47]. The force constants and intermolecular parameters were chosen in analogy to similar molecules already described by GROMOS.

The system's dimensions were carefully chosen to ensure an aqueous layer of at least 50 Å between the headgroups of the two opposing monolayers, therefore ensuring negligible interactions between lipid surfaces [48-49]. MD simulations were carried out up to 100 ns production run after the equilibration of the system. The images of MD simulations were made with visual molecular dynamics (VMD) [50] and Grace (xmgrace) [51] software.

Results and Discussion

Surface pressure (π)-Mean molecular area (Mma) isotherms of JO monolayers

Fig.1a shows π-Mma isotherms corresponding to two compression-expansion cycles of JO monolayers. Surface pressure grows smoothly upon compression, leading to an abrupt collapse followed by a *plateau*. This kind of collapse is characteristic of monolayers in a liquid-expanded (LE) phase collapsing at the equilibrium spreading pressure [22]. This behavior can be observed for example in pure [52] or complex TGs monolayers [19]. The equilibrium condition is evidenced by the absence of hysteresis along the compression-expansion cycles and contrasts with the non-equilibrium WE films following compression-expansion isocycles [16] where, instead of a unique monolayer pressure, a flattening of the isotherms occurred at π values that increased with successive isocycles, until the film reached an equilibrium. Here, the collapse was highly reproducible and corresponded to a LE phase (K_{max}= 30 mN/m). Besides, it occured at a low lateral pressure (π_C=2.2 ± 0.1 mN/m) and at a minimal mean molecular area (A_{min}) of 77 ± 2 Å^2/molecule, a relatively large value, considering the chain number (two) and the small polar group (monoester). This value differs to the previously reported A_{min} of 210 Å^2/molecule at a temperature (28 ºC) higher than the one set here (24 ºC). However, the present value is closer to those reported for other WEs at similar temperatures [13, 15].

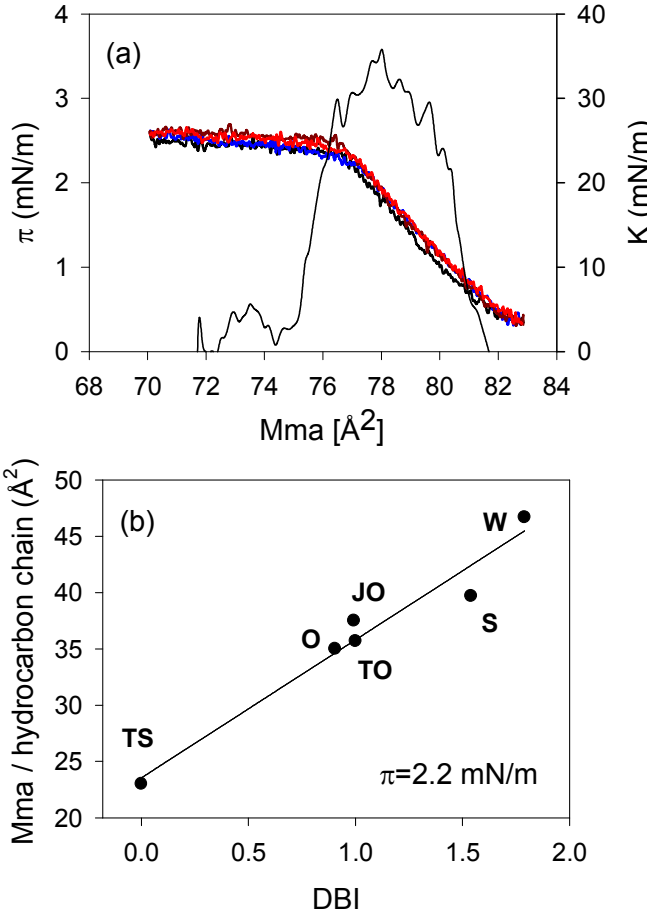

Fig.1. (a) Compression/expansion isotherms of JO (different color curves) and compressibility modulus (K) of the first compression. (b) Correlation between degree of unsaturation (DBI) and surface packing, expressed as area/hydrocarbon chain (HCA) of natural TGs (O, S and W), pure TGs (TS and TO) and JO. the straight line results from linear correlation analysis. R=0.979. K was calculated from Eq.2.

Because JO monolayers collapse at a very low surface pressure, it has been very difficult to find the spreading and compression conditions under which the isotherms are reproducible but, unlike other long chain WE films (both saturated and unsaturated), monolayer compression isotherms could be mapped. How can these different behaviors be explained? For saturated WE, the model proposed by Teixeira et al. [18] have suggested that the constraint for SS (a saturated WE, both C18:0 chains) to form stable monolayers at the air-water interface (adopting a hairpin-like structure) results from its low HLB. In this case the cost of hindering the polar group from being in contact with water is offset by the maximization of hydrophobic lateral interactions that can take place in an asymmetric bilayer (multilayer), being this the structure actually monitored in the compression isotherm (see the Introduction). Recently, WE films (BP, for behenil palmitoleate, i.e., C20:0/C16:1) were evaluated above and below their bulk melting point [15]. In the solid state, micron-scale surface aggregates were observed. Under isochoric heating BP spread over the surface forming a monolayer and increasing π up to a plateau of 2.3 mN/m at the BP bulk melting temperature (Tm). These authors suggested that when forming a monolayer, BP molecules adopt a hairpin configuration. However, their compression isotherms were performed at the Tm (where liquid monolayers and solid aggregates would coexist), precluding the existence of BP monolayers from their lift-off up to their collapse.

In the present work, isotherms of JO monolayers were recorded at a temperature (24 °C) well above the Tm of bulk JO (10 °C). Furthermore, as JO is a complex mixture of WE with a high proportion of unsaturated chains, the chain packing reached in an asymmetric bilayer would be less efficient than in SS and BP at maximizing hydrophobic interactions. Hence, the cost of hindering the polar headgroup from water would be proportionally higher, allowing the observation of compressible monolayers of JO with ester molecules possibly adopting only a hairpin-like structure. In order to test the hypothesis of a hairpin-like configuration, the properties of JO monolayers were contrasted with predictions taken from TGs monolayers, reasoning as follows. Since TGs molecules adopt a trident configuration at the interface and its polar head group is small compared to the volume occupied by the hydrophobic moiety, the properties of its hydrocarbon chains are determinant of its lateral packing and thus certain average parameters derived from the acyl composition may be correlated with its surface density. For instance, the degree of unsaturation of the acyl chains, described by the Double Bond Index (DBI_{TG}), is the parameter that best correlated with the Mma of TGs monolayers [19] obtained from the TG fraction of vegetable oils (olive, O; soybean, S and walnut, W). We hypothesize that if JO adopts a hairpin-like structure, then its

molecular packing should be governed by its chain composition as it occurs with TGs. Then, we interpolated the *DBI*-Mma values for JO in the correlation plot of *DBI* vs. Mma observed for the TGs O, S and W, whose *DBI* are: DBI_O=0.9054, DBI_S=1.5409 and DBI_W = 1.7862. The A_{min} per hydrocarbon chain of JO is 37.5 Å^2/chain at 2.2 mN/m, while for the different TGs analyzed at the same π these values are 35, 39.7 y 46.7 Å^2/chain for O, S and N, respectively. In Fig.1b the correlation between *DBI* and surface packing of TGs is shown, including the mentioned complex mixtures of TGs (O, S and W) and pure TGs taken from the literature, tristearin (TS) [53] and triolein (TO) [52]. It can be observed that *DBI*/Mma point values for JO are highly consistent with the correlation observed in TGs monolayers. Contrary to what would be expected from the relatively higher average length of JO chains compared with those of TGs considered in this analysis, Mma is close to the correlation line. Then, according to this first approach JO chain packing seems consistent with a hairpin-like structure.

Afterwards, we studied molecular properties of JO that should be affected by the polar head orientation and hydration at the interface. There are numerous studies with respect to the orientation of glycerol-ester-based lipids and other ester containing lipids, which describe the orientation of their chemical groups. In this regard, it has been highlighted the importance of differentiating esters in position 1 and 3 from that at position 2 of the glycerol backbone [54]. In this sense, the presence of only one ester group in the molecular structure of JO facilitates the analysis of the molecular orientation of WEs in the monolayer (if such monolayer is formed). The experiments that followed attempt to analyze what was the orientation at the interface of the monoester group of JO, seeking for an interpretation that allowed understanding the configuration of JO molecules at the interface at its maximal compression.

S*urface electrostatics of JO monolayers at the air-water interface.*

In Fig.2 π-Mma and ΔV-Mma experimental compression isotherms of JO monolayers are superimposed with a calculated $\mu_\perp$-Mma isotherm. Upon the monolayer compression, changes in ΔV, and consequently in the magnitude of the apparent dipole moment ($\mu_\perp$) of JO, could be sensed before the Wilhelmy plate method could registered an increase in π at the lift-off area (~100Å^2/molec).

Within the 200-140 Å^2/molec range the surface potential behaves erratically. An example of this is shown in Fig. 2a within the range 140-160 Å^2/molec .We think that this kind of fluctuations might be related to the fact that the monolayer is not well structured and that the air-water interface might not be homogeneously covered with JO molecules. At lower

molecular areas $\mu_\perp$ (and ΔV) increased monotonously from ~100 mD to ~550 mD. This regime remained until the monolayer reached the lift-off area and acquired molecular cohesion. At Mma ≤ ~100 Å^2/molec, both ΔV-Mma and $\mu_\perp$ - Mma exhibited new dipolar reorientations.

There are two chemical groups that may contribute to the observed ΔV in an ester of this type: the methyl terminals, which provide $\mu_\perp$ = 330-350 mD [55-56] and the ester bond. By assigning a dipole moment value for each component of the ester group and summing them up vectorially it was possible to explain the apparent dipole moment of a wide variety of long chain monoesters [14]. In the ester group, the $^{sp2}C{=}O$ and $^{sp3}C\text{-}O$ bonds (where sp^2 and sp^3 refers to the hybridizations of C atoms) would make the most significant contribution to the resultant molecular μ with values of 360 mD and 170 mD, respectively [14].

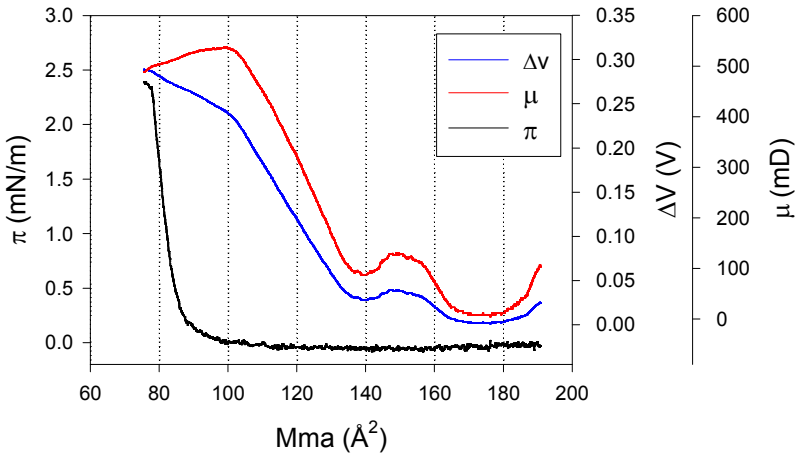

Fig.2. Compression isotherms of J showing π, ΔV and $\mu_\perp$ as a function of Mma. $\mu_\perp$ was calculated according to Eq. 3.

In the case of HP, a long chain WE mentioned in the *Introduction*, it was assumed that the bending of the alkyl chain for adopting a hairpin-like structure of the molecule would imply an arrangement where the $^{sp2}C{=}O$ dipole would be more parallel to the interface than the $^{sp3}C\text{-}O$ dipole and both in oppossed directions, compensating themselves and resulting on an almost null apparent dipole moment. Conversely, in the case of JO monolayer the calculated $\mu_\perp$ at maximal compression was far from zero. It is worth to note that, for the experiments with HP, data were obtained through the ionizing electrode method for ΔV measurements and monolayers were prepared over a 0.01 M HCl subphase. Furthermore, the analysis on HP was based on assumptions that neglected the contribution of both the terminal methyls and the water molecules oriented in the presence of the monolayer. Thus, it is not surprising that $\mu_\perp$ values for JO calculated in the present work are not comparable to that of HP which, in addition, came from the sole ΔV evidence found on the literature.

So, we followed up by comparing the surface behavior of JO with well-known models that make a general description of the behavior of aliphatic compounds. For this, the ΔV value was considered. The variation in ΔV of JO monolayer upon compression (Fig.2) includes an increase, starting from ΔV = 0 mV, that precedes the increase in lateral pressure. Oliveira and Bonardi [24], from studies on a variety of aliphatic compounds (acid, alcohol, methyl-ester, amine) observed a ΔV increase at a critical area of approximately twice the value of the lift-off molecular area. This behavior was ascribed to a sharp decrease in the local dielectric constant at the monolayer-water interface when the monolayer becomes structured. It would be a consequence of the removal of water molecules from the water-polar headgroup interface and is consistent with the critical area suggested by other techniques (Brewster Angle Microscopy, lateral conductance, UV reflection spectroscopy, ellipsometry) (ref. in [24]). In JO monolayers this increase started on average around 140 $Å^2$, followed by a decrease of the ΔV/Mma slope at a Mma (85-90 $Å^2$) lower than the lift-off area. This area range may be associated to the beginning of the molecular cohesion and the displacing of interfacial water.

At lower Mma, a LE structured monolayer shows a linear dependency of ΔV with respect to Mma. Such behavior was observed by Smaby and Brockman in a variety of aliphatic, mainly in long chain, glycerol-based esters (LCGE) [54]. This linearity does not imply proportionality between these variables. Through the analysis of the dependence of ΔV with 1/Mma of LE monolayers of these compounds, these authors propose the existence of an area-independent ΔV (termed ΔV_0), whose value is between 100 and 150 mV. This ΔV_0 is interpreted as a result of a "pool" of water which is oriented by the presence of the monolayer but not between the polar headgroups (i.e., it is not removed by the compression of the monolayer) [54]. We performed such analysis for JO monolayers obtaining an average ΔV_0 = 125 ± 30 mV. Hence, JO monolayer would be exerting the same effect that LCGE monolayers do on water molecules located between bulk water and the polar headgroups, suggesting that JO molecules are oriented in a manner similar to LCGE (polar headgroup facing water and hydrocarbon chains towards the air).

The maximal surface potential of the JO monolayer ΔV_{max} = 300 ± 40 mV was reached at the collapse point (Fig.2). This value was contrasted with the calculated with 3-layer capacitor Demchak-Fort $V_{D\text{-}F}$ model using the parameters listed in the Materials and Methods section [24], adapted to consider the contribution of 2 terminal methyls expected from a molecular configuration where both chains point toward the air (i.e., μ_3=660 mD, 330 mD for each of the terminal CH_3). To account for the variability of the A_{min} (the Mma taken at the

collapse point), data from 9 different JO monolayers were used for calculations. The resulting value was $V_{D\text{-}F}$ = 170 ± 20 mV. The experimental ΔV_{max} can be considered as the result of contributions dependent ($\Delta V_{D\text{-}F}$) and independent (ΔV_0) from the molecular density [57]. This yields a result similar to the value determined experimentally:

$$\Delta V_{max} = \Delta V_{D-F} + \Delta V_0 = (170 + 125)\ \text{mV} = 295\ \text{mV} \cong 300\ \text{mV}$$

The fact that ΔV_0 and ΔV_{max} are not mutually correlated, allows discarding the possibility that the variability in ΔV_{max} is due to the variability in ΔV_0 and supports the idea that these contributions are additive properties of the monolayer.

It is noteworthy that the acyl chains esterified on glycerolipids can acquire an extended (E) or bent or "kinked" (K) configurations when esterified at the sn-2 or at the sn-1 and sn-3 positions, respectively. This implies that the carbonyl *C=O* can be more parallel or perpendicular to the interface leading to μ_2/ε_2 of 132 ± 50 and 252 ± 27 mD for E and K configurations, respectively [54]. As the μ_2/ε_2 value assumed here for JO (173 mD) (which resulted in a good agreement between experimental and predicted ΔV_{max}) is an intermediate value between those exhibited by E and K configurations in glycerolipids, it is expectable that the $C=O$ of JO exhibit an intermediate orientation between both configurations. This was further evaluated by means of PM-IRRAS on JO monolayers and atomic-scale molecular dynamics simulations of a WE molecule representative of JO composition.

PM-IRRAS spectra on JO monolayers

PM-IRRAS spectra of JO monolayer are shown in Fig.3a and were recorded at different compression levels of the monolayer (pointed to by the arrows in Fig.3a, inset). The variation in the position (ν_{max}), expressed in wavenumber units (cm^{-1}), and in the PM-IRRAS signal intensity of the absorption peak corresponding to the carbonyl ***(C=O)*** and methylene (***C=C)*** groups are depicted as a function of compression (expressed as Mma) in Fig.3b and c, respectively. Upon monolayer compression, ν_{max} of ***C=O*** ($\nu_{C=O,max}$) increased reaching a maximum value between 120 and 77 $Å^2$ (≅0.5 mN/m) and decreased at smaller areas. This slight shift towards lower ν is indicative of a decrease in the hydration of ***C=O*** [25, 58-59] upon compression. The low value of $\nu_{C=O,max}$ for non-hydrated Jojoba oil (bulk oil) determined by regular FT-IR spectroscopy [10, 60], included in Fig.3b, suggests that JO films do not evidence non-hydrated ***C=O***. According to Δ*V* data, the onset of cohesion of JO molecules would take place at 120-140 $Å^2$. Then, this would explain the differences observed in $\nu_{C=O,max}$ between

non-hydrated bulk JO and the hydrated JO prior to the lift-off. Furthermore, there is no split in the ***C=O*** peak indicating that there is no coexistence of molecules with carbonyls with different hydration degrees. Since the values of $\nu_{C=O,max}$ are significantly higher than that of bulk JO, we can discard the possibility that molecules are organized in the fully extended configuration, in which case the carbonyls would be hidden from the water.

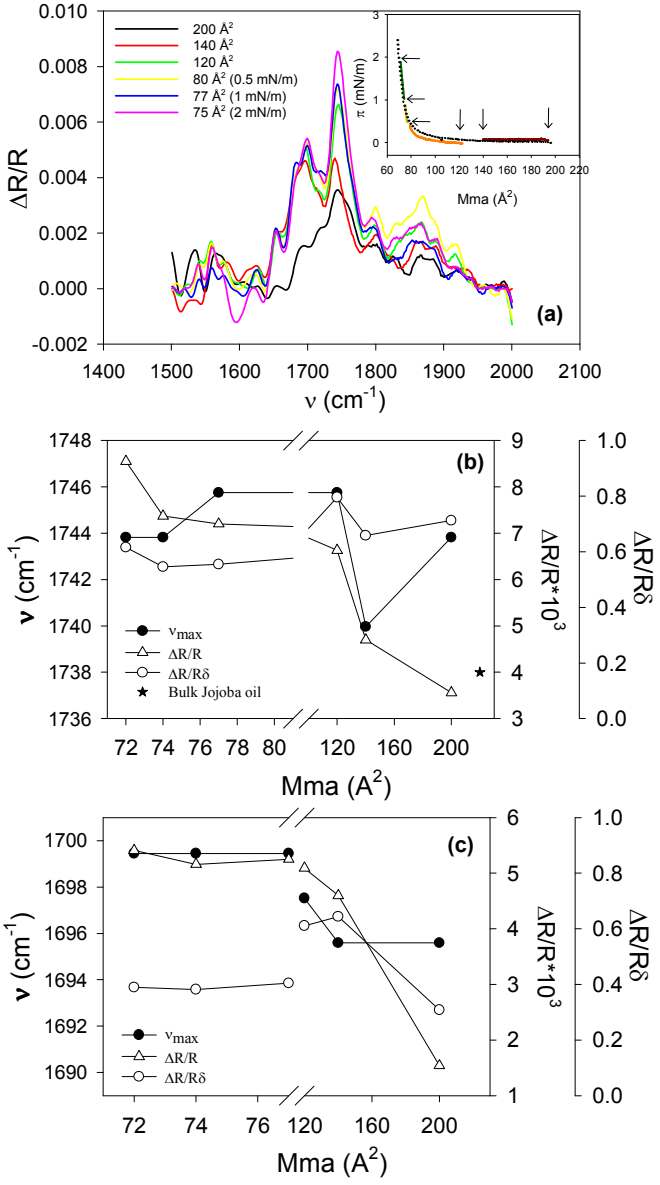

Fig.3. PM-IRRAS of J monolayers at the air-water interface. (a) Absorption spectra at different degrees of compression (indicated with arrows in the insert). (b, c) Parameters of the ***C=O*** and ***C=C*** vibrations, respectively. Namely, $\nu_{C=O,\ max}$ and $\nu_{C=C,\ max}$ ***C=O*** peaks wavenumbers; ΔR/R, PM-IRRAS normalized signal intensity; ΔR/R.δ, PM-IRRAS normalized signal intensity weighted by **JO** molecular surface density (δ). The star (★) correspond to ***C=O*** vibration frequency ν_{max} of bulk **JO** in the absence of water; for this point Mma is not relevant.

The magnitude of the normalized signal intensity (ΔR/R) of the ***C=O*** increased within the whole Mma range analyzed (Fig.3b). ΔR/R gives information about the combined effects of surface densities (δ) and reorientations of the absorbing dipoles. In turn, the magnitude of ΔR/R.δ of the ***C=O*** dipole (intensity change per unit of molecular surface density), which is only dependent on dipoles orientation, remained constant along compression (Fig.3b). Variations in ΔR/R.δ towards more positive values can be interpreted as the result of the ***C=O*** orientating more parallel to the interface. The opposite, i.e., a dipole orientating perpendicular to the interface, results in a negative signal. Moreover, it is considered that,

at an angle with respect to the normal to the interface θ~39°, the signal is canceled (known as the vanishing angle) [61]. So, taken together, these results indicated that the orientation of the ***C=O*** dipole was compatible with θ> 39° invariant with compression.

We assume that JO forms a LE structured monolayer at Mma~120 - 140 Å^2 thus, both parameters (ΔR/R and ν_{max}) should be analyzed with caution at larger areas. This is evident in the case of $\nu_{C=O,max}$, which exhibits great fluctuations at larger areas.

The peak at ~1700 cm^{-1}, may be assigned to the stretching of ***C=C*** bond, which in bulk (dehydrated) JO occurs between 1620 and 1680 cm^{-1} [60, 62]. The present higher values may be due to a higher polarity in the environment near this dipole (although ***C=C*** groups are mostly present between C9 and C13 atoms in the chains). This peak becomes more evident, increasing it´s wavenumber value as the monolayer is compressed up to the lift-off, after which both its position and normalized signal value remain constant, suggesting that at these densities JO chains adopt an arrangement that is maintained along the compression. This is in agreement with the onset of cohesion of JO molecules at 120-140 A2 (suggested above from ΔV).

Comparing both PM-IRRAS and ΔV techniques, it could be said that the decrease in the magnitude of $\mu_\perp$ of JO molecules when the monolayer is compressed below 90 Å^2 could not be explained as a result of reorientation of the carbonyl group towards a more parallel orientation with respect to the interface. It is worth noting that the disposition of the $^{sp^3}CO$ bond could not be observed by PM-IRRAS and it should not be ruled out a more vertical arrangement of it (which would contribute negatively to the dipole moment). On the other hand, a reorientation of the terminal methyls should also be considered, although it is expected that the compression of the monolayer increases the probability of finding the acyl chains, on average, in a vertical orientation, thus contributing to increase the modulus of $\mu_\perp$.

In order to get insights on the molecular basis of the monolayers organization we carried out molecular dynamics simulations.

Molecular Dynamics Simulations

As we have already discussed in the Materials and Methods section, JO is a complex mixture of different WEs. To carry out the simulations it is need to simplify the system. Hence, we have chosen one of the main molecular components of JO: the EE. Since monolayers simulations were run using the NVT ensemble, the area per lipid was tunned varying the

number of lipids in each monolayer. Two areas per lipid were selected: a) near the lift-off area range (100 Å^2) and b) preceding the monolayer collapse (80 Å^2), which are reference points in the experimental π-Mma compression isotherm. It is important to point out that the collapse area for EE could be a little shifted with respect to the corresponding to JO. The last 100 ns of the simulations production run trajectories were used to evaluate statistical properties of the systems

Electron density profiles

The interfacial ordering of the system is evaluated here by means of the electron density profile (EDP) normal to the monolayer. Fig.4 shows overimposed EDPs for both systems under investigation The electron density is being plotted against the *z* coordinate, where *z*=0 corresponds to the system center located in the middle of the aqueous phase. The EEs remain in a monolayer structure along the whole simulations time. We can see from Fig.4 the overall organization of the monolayers: the ester groups overlap with the water and the EE tails. The tails extend from the water to the vacuum phases.

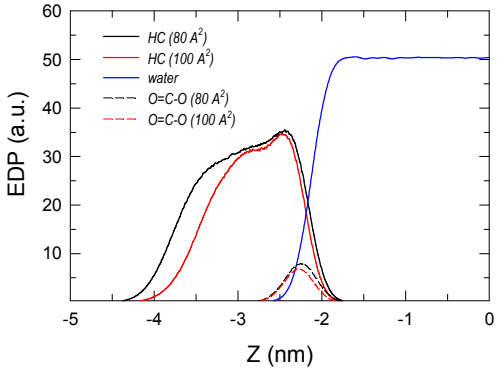

Fig.4: Electron Density Profile of the whole system. EE monolayer at 80Å^2 (black) and 100 Å^2 (red). Water (blue), ester group $\boldsymbol{O=C-O}$ (---;---). Hydrocarbon chains (*HC*) (—;—). The water and lipid heads are also shown. Vaccum towards the left side.

In order to describe the orientation of the lipid dipoles, we plotted in Fig.5 the organization of the four polar atoms of the ester groups, separately, at two areas per EE (80 A^2 and 100 A^2). In Figs.5a it can be observed a separation of the C_{sp2} and $O_{carbonilic}$ (C_{sp2}=O) peaks. On the other hand,

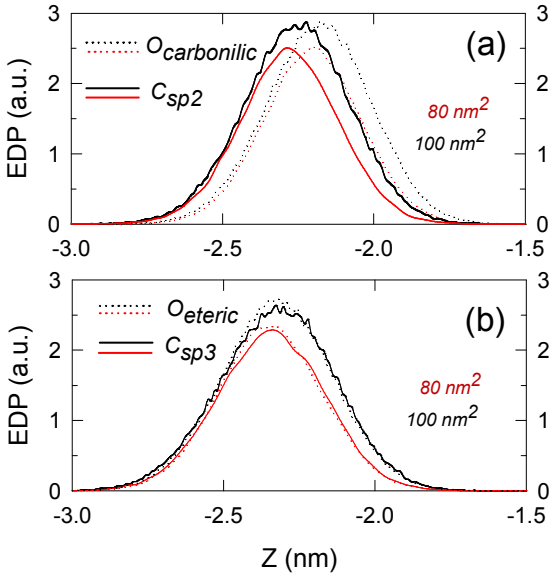

Fig.5. Density profiles of the constituent atoms of C_{sp2}=O and C_{sp3}-O vectors from EE monolayer with a molecular area=80 Å^2 (red lines) and 100 Å^2 (black lines). (a), $O_{carbonilic}$ and C_{sp2}; (b), C_{sp3}; and O_{eteric}. Water is at the right side.

in Figs.5b, it is shown a coincidence between the maximum of C_{sp3} and O_{eteric} (C_{sp3}-O), at both areas, indicating that, on average, they are laid parallel to the surface.

3.4.2 Polar head conformation

In order to investigate the orientation of the polar groups within the monolayer, we have calculated the angles, θ formed by each of the vectors C_{sp3}-O and C_{sp2}=O (going from the carbons C_{sp3} and C_{sp2} to the corresponding bonded O atoms) with respect to the bilayer normal.

———In Fig.6, we show the probability density, P(θ), for each of the vectors´ angles and at each area per lipid, normalized by the isotropic distribution, $P_{iso}(\theta)=1/2.\sin.\theta$. Integration of $P(\theta)/P^{iso}(\theta)$ over all angles yields unity. The orientation of the C_{sp3}-O and C_{sp2}=O associated vectors show peaks at ~90° and ~50°, respectively. These values were little affected by the surface area. The maximum probability was found for θ ~ 45°-50° for the C_{sp2}=O at both areas, in agreement with an invariable θ>39° angle interpreted from the PM-IRRAS (positive signal). Moreover, a constant θ~90° is observed for the C_{sp3}-O vector. Thus, variation in none of these vectors would account for the decrease in the global apparent dipole observed experimentally (Fig.2)

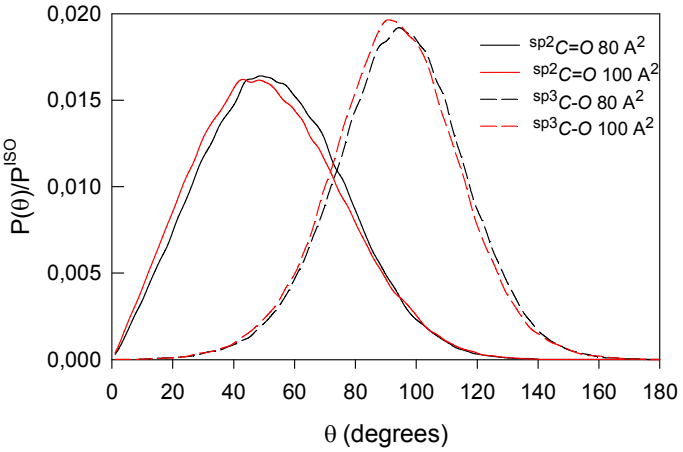

Fig.6. Vectors' angles. Monolayer molecular areas were set at 100 Å^2 (red) and 80Å^2 (black). Solid and dashed lines correspond to the ***C_{sp2}=O*** and ***C_{sp3}-O*** vectors, respectively.

Electrostatic potential across the interface

The electrostatic potential (ψ) across the interface, arising from the non-uniform distribution of dipoles, can be computed from a trajectory by evaluating the double integral of the charge density *ρ(z)* (Eq.5):

$$\psi(z)-\psi(-\infty)=-\int_{-\infty}^{z} dz' \int_{-\infty}^{z'} \rho(z'')\,dz''/\varepsilon_0 \qquad (5)$$

where the position $z=-\infty$ is far enough in the water bulk phase so that the field is zero and *ρ(z)* is the time averaged charge. The double integral of the charge density gives the electrostatic potential. The surface potential, ΔV, was estimated as the difference of electrostatic potential at the water phase respect to the air phase.

As discussed in Fig 2, this surface potential due to the presence of the monolayer varied towards positive values as the Mma decreases. Fig. 7 shows the potential profile, for both monolayers. We can see a drop in the potential profile as one goes from the water to the lipid tail region, more pronounced for the more compact monolayer in good agreement with experimental results. Although these comparisons can be considered only on a semiquantitative basis, the agreement between them is surprising, even thinking that we are simulating a simplified model of JO in a small box. On the other hand, if the increase in ΔV was due only to a change in the molecular surface density it would be expected a proportionality between ΔV and Mma (if at 100 Å^2 ΔV= 610 mV, then at 80 Å^2 ΔV should be 762 mV) which was not observed (610 and 715 mV at 100 and 80 Å^2, respectively). This lead to consider the possible contribution of an apparent dipole moment reorientation.

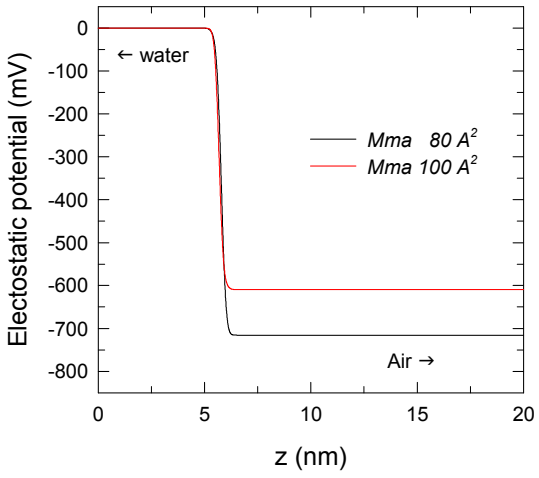

Fig.7. Electrostatic potential. 100 A^2 (red), 80 A^2 (black).

Since no significant dipole reorientation in the ester moiety was observed in the simulations (Fig.6), the apparent dipole reorientation derived from the experimental ΔV (Fig.2) and suggested by MD simulations (Fig.7) could be related to other factors, e.g. the hydrocarbon chains reorientation and/or water rearrangements.

Thus, the next step was to evaluate both alkyl and acyl chains structuring by means of the order parameter. It should be recalled that a chain disordering among compression, would lead to a negative contribution to the apparent dipole moment, in contrast with the Adam model[13].

Order parameter

The EE tail order parameter (S_{CD}) is a standard quantity to evaluate the structural order of acyl chains in lipid bilayers and monolayers, which can be obtained from deuterium NMR measurements. Fig 8 a and b shows the order parameter for the alkyl and acyl chains, respectively. An overall view shows a quite disorder lipid tails (a low parameter value means that CH_2 groups are not parallel to the bilayer normal).

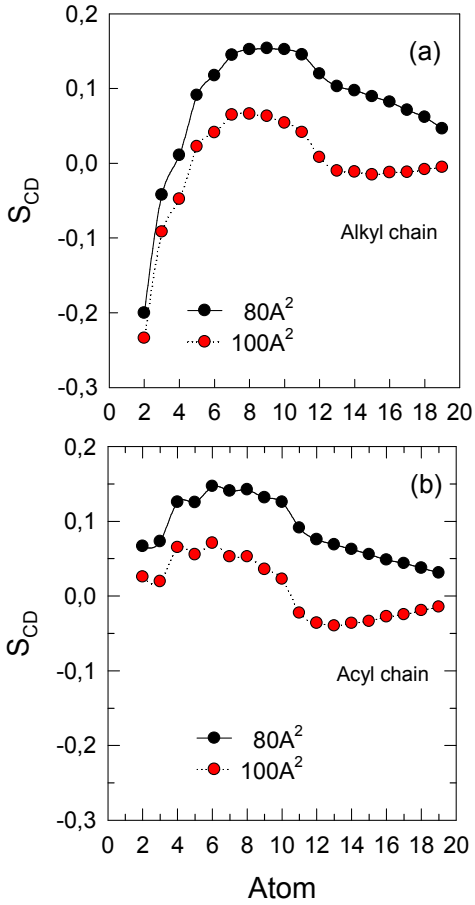

Fig.8. Order parameter of both alkyl (a) and acyl (b) chains at 80Å^2 (●) and 100Å^2.(●).

The order becomes maximal, but with opposite signs/orientations, towards C1 mainly in the alkyl chain and also around the central region in both alkyl and acyl chains between C6 and C8 in the former and extends from C4 to C10 in the latter. The S_{CD} near zero in the acyl chain suggests an important bending in this chain that precludes its ordering at C1. In both chains S_{CD} is higher at the lowest area/lipid. The disorder (trans-cis) around C11 decrease among diminishing the area per lipid (Fig.8). This indicates that both chains are being progressively orientated towards a more vertical disposition as they are compressed. However, S_{CD} values would be more consistent with a "V-shape" [63] rather than a hairpin configuration as proposed by Adam [13]

Moreover, this slight ordering tendency would explain neither the apparent dipole moment drop between 100 and 80 Å^2 observed in Fig.2 nor the slight reorientation of dipoles

suggested by the analyses done in the previous section. This strengthens the possibility that reorientation of a population of water molecules is taking place as suggested above.

Orientation of water molecules at the interface

In order to shed light on the water contribution to the surface potential, we calculated the angle (φ) orientation of water dipoles with respect to the bilayer normal from MD simulations. We considered the water molecules up to 10 Å from the interface. Fig. 9 shows the angle distribution, D(φ), in the range found as being of high frequency. We found two preferential orientation of water dipoles for both monolayers. This would be considered as the presence of two population of water molecules. In this way, one of them have a similar average value (~89º) for both studied cases, but with broader peak in the case of 80 $Å^2$. The other one presents a difference of 2º between both monolayers.

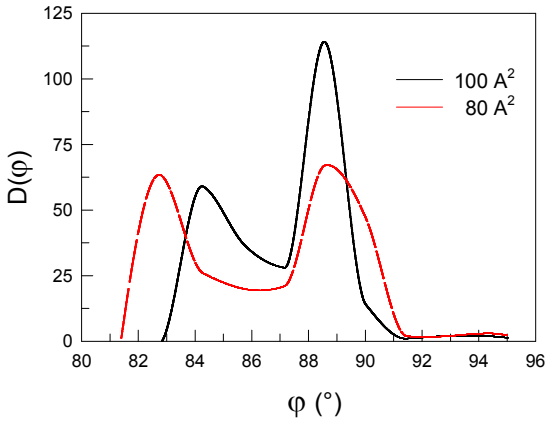

Fig. 9: Water dipole angle respect to the bilayer normal at: 80 $Å^2$ (red) and 100 $Å^2$ (black).

Taking into account the analysis of the other components which contribute to surface potential, we consider that the difference found for water orientation between both areas could lead a significant effect on the respective surface potential.

Conclusions

The present results confirm and contribute to understand how JO, a complex mixture of long chain unsaturated WE, is able to form stable monomolecular layers at the air-water interface. The monolayer compression isotherms are reproducible and, as opposed to other WE studied (pure and saturated long chain monoesters), exhibit a typical collapse that leads to a non-viscous liquid collapsed phase and a collapse pressure (π_c) corresponding to its equilibrium spreading pressure (π_e). The Mma of JO was comparable to those of pure monoesters forming LE monolayers and, when normalized per alkyl chain, correlated with an average parameter based on the degree of unsaturation of the hydrocarbon chains (DBI) previously applied to describe the collective behavior of a complex mixtures of TGs. This was the first indication that the "V-shape" configuration assumption allowed interpreting its surface behavior successfully.

Surface potential measurements showed that the formation of LE structured monolayers at low molecular densities is comparable to what was described for aliphatic compounds. This allowed us identifying a molecular density-independent component of ΔV (ΔV_0) , comparable to the calculated for a wide variety of long chain esters (including glycerol based esters), which was ascribed to a pool of water molecules immobilized at the monolayer-water interface. Thus, by assuming a "V-shape" configuration, we could properly reproduce the interfacial electrical properties of WE through a capacitor general model. This is the first experimental description of the electrostatic behavior of WE monolayers. In the literature, only theoretic reports of a null ΔV (based on short and saturated monoesters) can be found which are not accompanied by the experimental counterpart and were explained to be a consequence of the *C=O* group being parallel to the interface. Partially in agreement with this interpretation, the increase in the intensity of the ***C=O*** signal ($\Delta R/R.\delta$) in our PM-IRRAS measurements can be explained by a decrease in $\mu_\perp$ due to a reorientation of the ***C=O*** towards a more parallel direction with respect to the interface and is in the same direction of the small increase in the angle of the C_{sp2}=*O* vector derived from MD simulations but is far from being parallel to the interface ($\theta \sim 45°$). In addition, our data clearly demonstrated not a null but a positive ΔV due to the contributions of other molecular groups such us methyl terminals and of interfacial water (not to C_{sp3}-*O* vector whose orientational angle is ~90° according to MD).

In accordance with the predictions from Mma/DBI correlations, MD simulations also indicate that both hydrocarbon chains orient towards the vaccum space (equivalent to the air

phase). This required the bending of the alkyl chain as indicated by the S_{CD} negative values from C2 to C4. The first *in silico* description of WE at an air-water interface presented here supports its "V-shape" configuration and did not show a chain disordering during compression. Upon monolayer compression the reorientation of the headgroup dipoles derived from MD was slight and in the same direction as that indicated by PM-IRRAS while the analysis of $\nu_{C=O}$ in the PM-IRRAS spectra suggested a dehydration of the carbonyl group. Taken together MD, PM-IRRAS and the ΔV calculations from the 3-plates capacitor model, strongly suggest that the decrease in $\mu_{\perp}$ upon compression calculated from ΔV/Mma plots within the LE structured monolayer regime, cannot be explained mainly by the reorientations of polar head group dipoles but to the reorientation of an interfacial structured water molecular population.

The low stability of WE at the air-water interface (very low π_c) may be ascribed to the steric hindrance imposed by the bending of the alkyl chain, which impairs the packing of the hydrocarbon chains, and to the physicochemical properties of the alkyl esters as a whole (e.g low HLB). The latter is worsen with the withdrawing of ***C=0*** from the water phase upon compression, which induces a growing tendency of WE to escape from the interface and leads to the collapse of the monolayer at low π. So, the HLB for a molecule such as EE (1.5 according to Griffin method), is not enough to predict its stability at the air-water interface since it may change depending on the molecular conformation acquired.

Finally, it is important to emphasize that JO WE, even at low surface pressures ($\leq$ 2 mN/m), are able to form monolayers with the molecules in a conformation that is not the extended but another one with the hydrocarbon chains pointing to the air which we called a V-shape type. This indicates that they will be able to be part of a film compressed at higher pressures if mixed with other more stable surfactants. On the other hand, since it is demonstrated that they do not form multilayers or duplex films, it is expected that they have the ability to spread over a surface up to its collapse pressure. The important thing is not how much they will modify the tension of that surface, but the fact that they will be able to coat it all.

Acknowledgements

This work was financed by grants from SeCyT-Universidad Nacional de Córdoba, UBACYT Foncyt and Conicet

References

1. Benson, A. A.; Lee, R. F., Wax esters: major marine metabolic energy sources. *Biochemical Journal* **1972,** *128* (1), 10P-10P.
2. Fixter, L. M.; Nagi, M. N.; Mccormack, J. G.; Fewson, C. A., Structure, Distribution and Function of Wax Esters in Acinetobacter calcoaceticus. *Microbiology* **1986,** *132* (11), 3147-3157.
3. Gibbs, A. G., Lipid melting and cuticular permeability: new insights into an old problem. *J Insect Physiol* **2002,** *48* (4), 391-400.
4. Kerstiens, G., Water transport in plant cuticles: an update. *Journal of experimental botany* **2006,** *57* (11), 2493-9.
5. Gibbs, A. G., Thermodynamics of cuticular transpiration. *Journal of Insect Physiology* **2011,** *57* (8), 1066-1069.
6. Samuels, L.; Kunst, L.; Jetter, R., Sealing plant surfaces: cuticular wax formation by epidermal cells. *Annual review of plant biology* **2008,** *59*, 683-707.
7. Paananen, R. Surface behavior of anti-evaporative tear film wax esters. Master´s thesis, University of Helsinsky, Helsinsky, 2014.
8. Iven, T.; Herrfurth, C.; Hornung, E.; Heilmann, M.; Hofvander, P.; Stymne, S.; Zhu, L.-H.; Feussner, I., Wax ester profiling of seed oil by nano-electrospray ionization tandem mass spectrometry. *Plant Methods* **2013,** *9*, 24-24.
9. Perillo, M. A.; Maestri, D. M., Surface behavior of jojoba oil alone or in mixtures with soybean oil. *Colloids and Surfaces A: Physicochemical and Engineering Aspects* **2005,** *256* (2-3), 199-205.
10. Shah, S. N.; Sharma, B. K.; Moser, B. R.; Erhan, S. Z., Preparation and Evaluation of Jojoba Oil Methyl Esters as Biodiesel and as a Blend Component in Ultra-Low Sulfur Diesel Fuel. *BioEnergy Research* **2010,** *3* (2), 214-223.
11. Lardizabal, K. D.; Metz, J. G.; Sakamoto, T.; Hutton, W. C.; Pollard, M. R.; Lassner, M. W., Purification of a jojoba embryo wax synthase, cloning of its cDNA, and production of high levels of wax in seeds of transgenic arabidopsis. *Plant physiology* **2000,** *122* (3), 645-55.
12. Dyer, J. M.; Stymne, S.; Green, A. G.; Carlsson, A. S., High-value oils from plants. *Plant J* **2008,** *54* (4), 640-55.
13. Adam, N. K., The Structure of Surface Films. Part XIV. Some Esters of Fatty Acids. Evidence of Flexibility in the Long Chains. *Proceedings of the Royal Society of London. Series A, Containing Papers of Mathematical and Physical Character* **1930,** *Vol. 126* (802), 366-372
14. Alexander, A. E.; Schulman, J. H., Orientation in Films of Long-Chain Esters. *Proceedings of the Royal Society of London. Series A, Mathematical and PhysicalSciences* **1937,** *161* (904), 115-127.
15. Paananen, R. O.; Rantamäki, A. H.; Holopainen, J. M., Antievaporative Mechanism of Wax Esters: Implications for the Function of Tear Fluid. *Langmuir* **2014,** *30* (20), 5897-5902.
16. Schuett, B. S.; Millar, T. J., Lipid Component Contributions to the Surface Activity of Meibomian LipidsLipid Contributions to the Activity of Meibomian Lipids. *Investigative Ophthalmology & Visual Science* **2012,** *53* (11), 7208-7219.
17. Caruso, B. Biophysics of the self-assembly of complex lipidic mixtures. Interaction with a soluble enzyme and modulation of its activity. Doctoral Thesis. National University of Córdoba, Córdoba, Argentina, 2011.

18. Teixeira, A. C.; Brogueira, P.; Fernandes, A. C.; Goncalves da Silva, A. M., Phase behaviour of binary mixtures involving tristearin, stearyl stearate and stearic acid: thermodynamic study and BAM observation at the air-water interface and AFM analysis of LB films. *Chemistry and physics of lipids* **2008,** *153* (2), 98-108.
19. Caruso, B.; Maestri, D. M.; Perillo, M. A., Phosphatidylcholine/vegetable oil pseudo-binary mixtures at the air-water interface: predictive formulation of oil blends with selected surface behavior. *Colloids Surf B Biointerfaces* **2010,** *75* (1), 57-66.
20. Perillo, M. A.; Polo, A.; Guidotti, A.; Costa, E.; Maggio, B., Molecular parameters of semisynthetic derivatives of gangliosides and sphingosine in monolayers at the air-water interface. *Chemistry and physics of lipids* **1993,** *65* (3), 225-38.
21. Garcia, D. A.; Perillo, M. A., Flunitrazepam-membrane non-specific binding and unbinding: two pathways with different energy barriers. *Biophys Chem* **2002,** *95* (2), 157-64.
22. Gaines Jr., G. L., *Insoluble monolayers at liquid-gas interfaces*. John Wiley & Sons, Inc: New York, 1966.
23. Dynarowicz-Latka, P.; Dhanabalan, A.; Oliveira, O. N., Jr., Modern physicochemical research on Langmuir monolayers. *Adv Colloid Interface Sci* **2001,** *91* (2), 221-93.
24. Oliveira, O. N.; Bonardi, C., The Surface Potential of Langmuir Monolayers Revisited. *Langmuir* **1997,** *13* (22), 5920-5924.
25. Blaudez, D.; Turlet, J.-M.; Dufourcq, J.; Bard, D.; Buffeteau, T.; Desbat, B., Investigations at the air/water interface using polarization modulation IR spectroscopy. *Journal of the Chemical Society, Faraday Transactions* **1996,** *92* (4), 525-530.
26. Buffeteau, T.; Desbat, B., Thin-Film Optical Constants Determined from Infrared Reflectance and Transmittance Measurements. *Appl. Spectrosc.* **1989,** *43* (6), 1027-1032.
27. Martini, M. F.; Disalvo, E. A.; Pickholz, M., Nicotinamide and picolinamide in phospholipid monolayers. *Int.J.Quantum Chem.* **2012,** *112*, 3289-3295.
28. de Moura, A. F.; Trsic, M., Molecular Dynamics Simulation of a Perylene-Derivative Langmuir Film. *The Journal of Physical Chemistry B* **2005,** *109* (9), 4032-4041.
29. Li, Z.; Cranston, B.; Zhao, L.; Choi, P., Molecular dynamics studies of the stability of water/n-heptane interfaces with adsorbed naphthenic acids. *The journal of physical chemistry. B* **2005,** *109* (44), 20929-37.
30. Nielsen, S. O.; Lopez, C. F.; Moore, P. B.; Shelley, J. C.; Klein, M. L., Molecular Dynamics Investigations of Lipid Langmuir Monolayers Using a Coarse-Grain Model. *The Journal of Physical Chemistry B* **2003,** *107* (50), 13911-13917.
31. Pickholz, M.; Oliveira, O. N.; Skaf, M. S., Molecular Dynamics Simulations of Neutral Chlorpromazine in Zwitterionic Phospholipid Monolayers. *The Journal of Physical Chemistry B* **2006,** *110* (17), 8804-8814.
32. Lairion, F.; Disalvo, E. A., Effect of arbutin on the dipole potential and area per lipid of ester and ether phosphatidylcholine and phosphatidyl ethanolamine monolayers. *Biochimica et Biophysica Acta (BBA) - Biomembranes* **2007,** *1768* (3), 450-456.
33. Lapin, N.; Seitz, O.; Chabal, Y. J., Chapter 4 - Infrared analysis of biomolecule attachment to functionalized silicon surfaces. In *Biointerface Characterization by Advanced IR Spectroscopy*, Elsevier: Amsterdam, 2011; pp 83-113.
34. Rand, R. P.; Fuller, N.; Parsegian, V. A.; Rau, D. C., Variation in hydration forces between neutral phospholipid bilayers: evidence for hydration attraction. *Biochemistry* **1988,** *27* (20), 7711-7722.
35. Berendsen, H. J. C.; van der Spoel, D.; van Drunen, R., GROMACS: A message-passing parallel molecular dynamics implementation. *Computer Physics Communications* **1995,** *91* (1), 43-56.

36. Hess, B.; Kutzner, C.; van der Spoel, D.; Lindahl, E., GROMACS 4: Algorithms for Highly Efficient, Load-Balanced, and Scalable Molecular Simulation. *Journal of Chemical Theory and Computation* **2008,** *4* (3), 435-447.
37. Van Der Spoel, D.; Lindahl, E.; Hess, B.; Groenhof, G.; Mark, A. E.; Berendsen, H. J., GROMACS: fast, flexible, and free. *Journal of computational chemistry* **2005,** *26* (16), 1701-18.
38. Oostenbrink, C.; Villa, A.; Mark, A. E.; van Gunsteren, W. F., A biomolecular force field based on the free enthalpy of hydration and solvation: the GROMOS force-field parameter sets 53A5 and 53A6. *Journal of computational chemistry* **2004,** *25* (13), 1656-76.
39. Berendsen, H. J. C.; Postma, J. P. M.; van Gunsteren, W. F.; Hermans, J., Interaction Models for Water in Relation to Protein Hydration. In *Intermolecular Forces: Proceedings of the Fourteenth Jerusalem Symposium on Quantum Chemistry and Biochemistry Held in Jerusalem, Israel, April 13–16, 1981*, Pullman, B., Ed. Springer Netherlands: Dordrecht, 1981; pp 331-342.
40. Darden, T.; York, D.; Pedersen, L., Particle mesh Ewald: An N·log(N) method for Ewald sums in large systems. *The Journal of Chemical Physics* **1993,** *98* (12), 10089-10092.
41. Essmann, U.; Perera, L.; Berkowitz, M. L.; Darden, T.; Lee, H.; Pedersen, L. G., A smooth particle mesh Ewald method. *The Journal of Chemical Physics* **1995,** *103* (19), 8577-8593.
42. Berendsen, H. J. C.; Postma, J. P. M.; Gunsteren, W. F. v.; DiNola, A.; Haak, J. R., Molecular dynamics with coupling to an external bath. *The Journal of Chemical Physics* **1984,** *81* (8), 3684-3690.
43. Martinez, J. M.; Martinez, L., Packing optimization for automated generation of complex system's initial configurations for molecular dynamics and docking. *Journal of computational chemistry* **2003,** *24* (7), 819-25.
44. Becke, A. D., Density‐functional thermochemistry. III. The role of exact exchange. *The Journal of Chemical Physics* **1993,** *98* (7), 5648-5652.
45. M. J. Frisch, G. W. T., H. B. Schlegel, G. E. Scuseria, M. A. Robb, J.R. Cheeseman, V. G. Zakrzewski, J. J. A Montgomery, R. E. Stratmann, J.C. Burant, S. Dapprich, J. M. Millam, A. D. Daniels, K. N. Kudin, M. C. Strain, O. Farkas, J. Tomasi, V. Barone, M. Cossi, R. Cammi, B. Mennucci, C. Pomelli, C. Adamo, S. Clifford, J. Ochterski, G. A. Petersson, P. Y. Ayala, Q. Cui, K. Morokuma, D. K. Malick, D. Rabuck, K. Raghavachari, J.B. Foresman, J. Cioslowski, J. V. Ortiz, B. B. Stefanov, G. Liu, A. Liashenko, P. Piskorz, I. Komaromi, R. Gomperts, R. L. Martin, D. J. Fox, T. Keith, M. A. Al-Laham, C. Y. Peng, A. Nanayakkara, C. Gonzalez, M. Challacombe, P. M. W. Gill, B. Johnson, W. Chen, M. W. Wong, J. L. Andres, C. Gonzalez, M. Head-Gordon, E. S. Replogle, J. A. Pople, , GAUSSIAN98 (Revision A.7);. Gaussian Inc.:: Pittsburgh, PA, 1998.
46. Chandra, S. U.; A., K. P., An approach to computing electrostatic charges for molecules. *Journal of computational chemistry* **1984,** *5* (2), 129-145.
47. Piotr, C.; Peter, K., On the use of electrostatic potential derived charges in molecular mechanics force fields. The relative solvation free energy of cis‐ and trans‐N‐methyl‐acetamide. *Journal of computational chemistry* **1991,** *12* (10), 1232-1236.
48. Feller, S. E.; Zhang, Y.; Pastor, R. W., Computer simulation of liquid/liquid interfaces. II. Surface tension‐area dependence of a bilayer and monolayer. *The Journal of Chemical Physics* **1995,** *103* (23), 10267-10276.
49. Feller, S. E.; Zhang, Y.; Pastor, R. W.; Brooks, B. R., Constant pressure molecular dynamics simulation: The Langevin piston method. *The Journal of Chemical Physics* **1995,** *103* (11), 4613-4621.

50. Humphrey, W.; Dalke, A.; Schulten, K., VMD: Visual molecular dynamics. *Journal of Molecular Graphics* **1996,** *14* (1), 33-38.
51. Stambulchik, E., Grace. 1998–2000 [retrieved June 20, 2009].
52. Mitsche, M. A.; Wang, L.; Small, D. M., Adsorption of egg phosphatidylcholine to an air/water and triolein/water bubble interface: use of the 2-dimensional phase rule to estimate the surface composition of a phospholipid/triolein/water surface as a function of surface pressure. *The journal of physical chemistry. B* **2010,** *114* (9), 3276-84.
53. Zdravkova, A. N.; van der Eerden, J. P. J. M., Structure and dynamics of Langmuir–Blodgett tristearin films: Atomic force microscopy and theoretical analysis. *Journal of Crystal Growth* **2006,** *293* (2), 528-540.
54. Smaby, J. M.; Brockman, H. L., Surface dipole moments of lipids at the argon-water interface. Similarities among glycerol-ester-based lipids. *Biophysical journal* **1990,** *58* (1), 195-204.
55. Oliveira; O. N, J. R.; Taylor; D, M.; Lewis; T, J.; Salvagno; S; Stirling; C. J, M., *Estimation of group dipole moments from surface potential measurements on Langmuir monolayers*. Chemical Society, Faraday Division: London, ROYAUME-UNI, 1989; Vol. 85.
56. Vogel, V.; Möbius, D., Local surface potentials and electric dipole moments of lipid monolayers: Contributions of the water/lipid and the lipid/air interfaces. *Journal of Colloid and Interface Science* **1988,** *126* (2), 408-420.
57. Brockman, H., Dipole potential of lipid membranes. *Chem Phys Lipids* **1994,** *73* (1-2), 57-79.
58. Estrela-Lopis, I.; Brezesinski, G.; Möhwald, H., Dipalmitoyl-Phosphatidylcholine/Phospholipase D Interactions Investigated with Polarization-Modulated Infrared Reflection Absorption Spectroscopy. *Biophysical journal* **2001,** *80* (2), 749-754.
59. Huo, Q.; Dziri, L.; Desbat, B.; Russell, K. C.; Leblanc, R. M., Polarization-Modulated Infrared Reflection Absorption Spectroscopic Studies of a Hydrogen-Bonding Network at the Air−Water Interface. *The Journal of Physical Chemistry B* **1999,** *103* (15), 2929-2934.
60. Harry-O'kuru, R. E.; Mohamed, A.; Abbott, T. P., Synthesis and characterization of tetrahydroxyjojoba wax and ferulates of jojoba oil. *Industrial Crops and Products* **2005,** *22* (2), 125-133.
61. Blaudez, D.; Castano, S.; Desbat, B., Chapter 2 - PM-IRRAS at liquid interfaces A2 - Pradier, C.M. In *Biointerface Characterization by Advanced IR Spectroscopy*, Chabal, Y. J., Ed. Elsevier: Amsterdam, 2011; pp 27-55.
62. Coates, J., Interpretation of Infrared Spectra, A Practical Approach. In *Encyclopedia of Analytical Chemistry*, John Wiley & Sons, Ltd: 2006.
63. Schroeter, A.; Stahlberg, S.; Skolova, B.; Sonnenberger, S.; Eichner, A.; Huster, D.; Vavrova, K.; Hau; Dobner, B.; Neubert, R. H. H.; Vogel, A., Phase separation in ceramide[NP] containing lipid model membranes: neutron diffraction and solid-state NMR. *Soft Matter* **2017,** *13* (10), 2107-2119.

TABLE OF CONTENTS IMAGE